

# CIRCULAR TARGET OBSERVATION OF POINT CLOUD USING LASER REFLECTION INTENSITY BY AN UNMANNED AERIAL VEHICLE EQUIPPED WITH A LASER SCANNER

Kazuya Nakano

Geospatial Information Laboratory, AERO ASAHI CORPORATION,  
3-14-4, Minamidai, Kawagoe, Saitama 350-1165, Japan - kazuya-nakano@aeroasahi.co.jp

Commission II, WG II/3

**KEY WORDS:** Circular Target Observation, Inhomogeneous Density Point Cloud, Unmanned Aerial Vehicles (UAVs), Laser Reflection Intensity.

## ABSTRACT:

Unmanned aerial vehicles (UAVs) equipped with laser scanners have been widely used for various purposes, such as in construction sites, forestry, and disaster management, as they can obtain high density point clouds with millimeter to centimeter scale accuracy. However, systematic errors in the height of a UAV relative to the earth's surface may occur owing to the method of direct georeferencing using the global navigation system satellite (GNSS) and inertial measurement unit (IMU). Therefore, to enable highly accurate surveying, adjustments must be made using ground control points. However, interpreting the ground control points of a discrete, inhomogeneous density point cloud requires a high degree of skill and effort. In this study, a high-end UAV laser scanner was used to obtain the point clouds of a site using a white circular target enclosed within a black frame in a measurement setup of 500 points/m<sup>2</sup>. The center coordinates of the circle, calculated using the conventional and proposed methods, were evaluated qualitatively and quantitatively. As a result, the average of 10 error distances was found to be 0.028 m for the weighted center of gravity method, 0.014 m for the fitting circle equation method, and 0.008 m for the proposed method. These results corresponded to one-fifth to one-half of the 0.045-m point intervals of the measurement plan. Thus, using the reflection intensity of point clouds, the circular target observation could be performed.

## 1. INTRODUCTION

Unmanned aerial vehicles (UAVs) equipped with laser scanners are used at construction sites to improve the productivity of all production processes and acquire highly accurate dense point clouds with an RMSE value less than  $\pm 0.02$  m of the height of the check points (Nakano et al., 2020). Although the UAV laser scanner is an extremely useful tool, it may feature systematic errors in its height relative to the earth's surface owing to the application of direct georeferencing method using the global navigation system satellite (GNSS) and inertial measurement unit (IMU). Therefore, it is necessary to make adjustments using ground control points for achieving highly accurate surveying. There have been many studies on target detection and registration using terrestrial laser scanners (see Akca 2003, Medić et al. 2019). The dense point clouds of UAV laser scanners are similar to those of terrestrial laser scanners, but their working principle is similar to that of airborne laser scanners. Csanyi et al. (2007) showed that an accuracy of 5 points/m<sup>2</sup> could be obtained for a circular target of radius 1 m using airborne laser scanners. Furthermore, Cramer et al. (2018) used UAV laser scanners and dense image matching to perform highly accurate measurements for monitoring the deformation in and around ship locks; they achieved an accuracy of more than 0.005 m using 0.27-m diameter checkerboard targets. Nurunnabi et al. (2018) presented robust statistical approaches for circle fitting in an incomplete laser scanning point cloud, such as in a partial arc. Four existing and two proposed methods of circle fitting were evaluated using the simulated data of arcs and circles with outliers and realistic laser scanning data, namely those of the terrestrial, airborne, and mobile laser scanners. However, the circle fitting was done for point clouds with spatially independent circle features; in the section on street lamps, the point cloud of the circle was obtained

using the boundary detection algorithm proposed by Belton and Lichti (2006). Davidson et al. (2019) analyzed the ground control targets for UAV laser scanners using gable roof targets and circular targets and obtained several findings pertaining to the determination of circular targets with black and white contrast for speedy identification. Furthermore, the circular targets were easier and faster to set out and were subsequently recorded. The gable roof targets enabled the visual identification of strip misalignment in a homogenous landscape. Although these targets are useful as they have a high interpretability owing to their shape, rigidity is required relative to their size for enabling interpretation and they have low portability. It should be noted that the ground control points have a significant impact on the survey results in terms of their accuracy. However, compared to images, point clouds are discrete and inhomogeneous, and thus, the task of observing them manually requires a high level of skill and effort. As discussed earlier, a theoretical accuracy of the measurement point was achieved considering the error propagation in the evaluation of the UAV laser scanner (Nakano et al., 2020). The observation equation used therein incorporated various parameters, such as the position of the GNSS, attitude of the IMU, and the distance and scan angular values of the laser scanner, boresight matrix, and lever arm. However, it was not possible to include the target observation accuracy of the point cloud as an observation equation parameter. To formulate the target observations of the point cloud, we evaluated the proposed and conventional observation methods, focusing on the portable plane circular target of point clouds using the reflection intensity.

## 2. TARGET OBSERVATION METHOD

Observing a high-contrast target using reflection intensity is easier when the density of points is sufficiently high and the

target is large relative to the point intervals. Under ideal conditions, the center coordinates of a circular target are expected to be almost the same as the center of gravity coordinates of the point cloud in the target area. Thus,

$$\begin{aligned} x_c &= \frac{\sum_{i=1}^n (x_i \cdot T \cdot g_i)}{\sum_{i=1}^n (T \cdot g_i)}, \\ y_c &= \frac{\sum_{i=1}^n (y_i \cdot T \cdot g_i)}{\sum_{i=1}^n (T \cdot g_i)}, \\ T &= \begin{cases} 0 & \text{for } g < t \\ 1 & \text{for } g \geq t \end{cases} \end{aligned} \quad (1)$$

where  $(x_c, y_c)$  are the center coordinates of the circular target,  $n$  is the number of processed points, and  $g_i$  is the grey value at the point position  $(x_i, y_i)$ . The decision function  $T$  was used to decide whether a point would be used for the calculation.  $T$  was defined by the grey value threshold  $t$ .

The coordinates  $(x_c, y_c)$  indicate the position of the center of gravity of the point cloud, calculated from Equation (1) using the centroid methods of the digital image (Luhmann et al., 2014). Therefore, the calculation of the center of gravity of the point cloud using the reflection intensity could be used as an observation method in the case of homogeneity of the point density in the images.

The center coordinates  $(x_c, y_c)$  of the circular target could also be calculated by using the circumference points and applying the least squares method to the Circle Equation (2) in the circle of the geometric elements (Luhmann et al., 2014).

$$(x - x_c)^2 + (y - y_c)^2 = r^2, \quad (2)$$

where  $(x, y)$  are the coordinates of the circumference points, and  $r$  is the radial that depends on the target size.

However, owing to the sway of the aircraft caused by wind and other factors, the flight of the UAV may not proceed as planned, and the homogeneity of the point density may not be obtained. Hence, highly accurate observations would not be possible by performing simple calculations. Moreover, it should be noted that the coordinates of the obtained point cloud would not necessarily be on the boundary of the target circle. Thus, the logic of human observation of the point clouds should be considered as a method of selection and weighting using reflection intensity for realizing the circular target observation. Accordingly, the proposed workflow, shown in Figure 1, may be used for this purpose. The workflow procedure comprised the following detailed steps.

1. The initial target positions would be given by the coordinates with different methods, such as GNSS and from approximate manual observations.
2. The point cloud around the target position would be collected by considering the error caused by the direct georeferencing method.
3. The height noises exceeding the specification measurement error would be removed by deviating from the plane equation.
4. The approximate positions of the target in the point cloud would be calculated by a weighted center of gravity method using the coordinates and reflection intensity. The grey value threshold  $t$  was to be determined using the Otsu threshold method (Otsu, 1979) because the reflection intensity would vary depending on the situation.
5. The circumference coordinates of the circle would be obtained by dividing the point cloud around the approximate

position into Delaunay triangulations and using the reflection intensity.

6. The center coordinates of the circle would be calculated by the least squares method of the circle equation using the circumference coordinates.
7. The point cloud near the circumference of the calculated center would be adopted or rejected based on the reflection intensity.
8. A movement vector would be obtained from the circumference coordinates for calculating the center coordinates.
9. The center of the circle would be moved by applying the summation of the movement vectors.
10. The center of the circle would be iteratively calculated until the amount of movement was less than the threshold value.

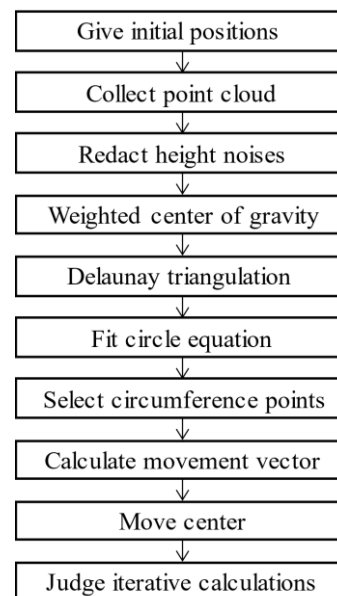


Figure 1. Proposed workflow.

### 3. DATA ACQUISITION

The acquired point cloud was used for performing boresight calibration of the UAV equipped with a laser scanner having high-end specifications, as shown in Table 1. In particular, the distance accuracy and scan rate of this laser scanner unit were  $\pm 5$  mm and 1000 kHz, respectively. Based on these specifications and the measurement settings (Table 2), the point density of the plan was 500 points/m<sup>2</sup>.

Item	Specifications
GNSS/IMU	Applanix AP20
Positioning accuracy	0.03–0.06 m
Roll, Pitch	0.015°
Heading	0.035°
Laser scanner	RIEGL VUX-1HA
Pulse repetition rate	300–1000 kHz
Scan rate	50–250 Hz
Maximum measuring range	235–420 m with an 80% reflectance
Distance accuracy	$\pm 5$ mm
Return	5 real-time waveform analysis
Laser class	I
Total Weight	ca. 4.5 kg

Table 1. Laser scanner specifications.

Item	Setting
Flight height	75 m
Flight speed	4.3 m/s
Pulse rate	1017.0 kHz
Scan rate	96.5 Hz
Flight speed	4.3 m/s
Along track intervals	0.045 m
Perpendicular intervals	0.045 m
Scan angle	90°
Density	500 points/m <sup>2</sup>

**Table 2.** Measurement plan settings.

The data of five circular targets were acquired from two courses of measurements, which included the misalignment before performing the boresight calibration. This ensured that the target positions in the point clouds in each course did not exist in the same position.

Figures 2 and 3 show the site situation of the data acquisition in grey scale point cloud using the laser reflection intensity and in true color point cloud using structure from motion (SfM) / multi-view stereo (MVS) with photo-images for reference of interpretation, respectively. T1–T5 in Figures 2 and 3 indicate the target locations. The white car included in Figure 3 does not exist in Figure 2 because of the difference in measurement times.

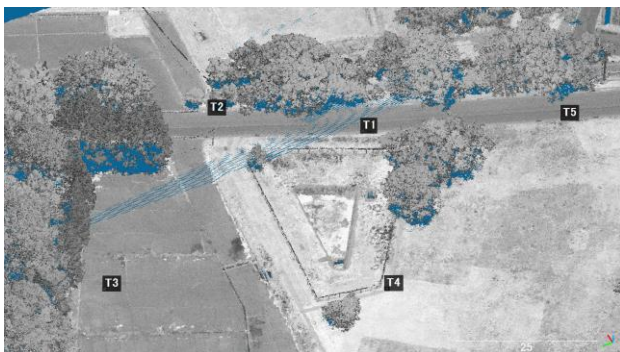


**Figure 2.** Situation of data acquisition using reflection intensity.



**Figure 3.** Site situation in true color point cloud.

Each circular target was shaped as a white circle enclosed within a black frame with the diameter of the white circle being either 0.50 m or 0.45 m, as shown in Figure 4. The figure shows an ortho-image generated using SfM/MVS. The white circle in the figure is clearly visible. However, the black frame appears whitish owing to the halation caused by the sun's altitude.



**Figure 4.** Ortho-image of the circular target 4.

Figures 5–8 show the typical target acquisition situations with point clouds obtained using the reflection intensity. The white points in the figure indicate strong reflective intensity, whereas the black ones indicate weak intensity.

The point cloud in the target area obtained using reflection intensity had a similar appearance as Target 4 of Course 1 in a stable measurement setting, as shown in Figure 5. However, there were instances of missing measurements for the black frame in the case of Target 2 of Course 1 shown in Figure 6. From the figure, it is evident that fitting the black frame with the missing measurements was difficult. Furthermore, the contrast between black and white was diminished owing to the scan angle in the case of Target 3 of Course 1 shown in Figure 7.

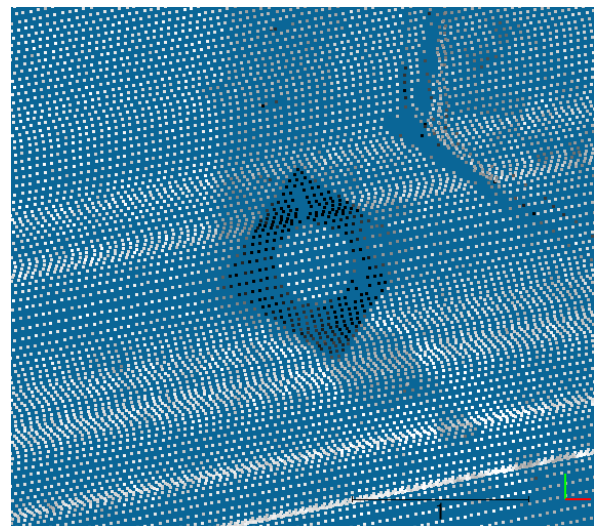


**Figure 5.** Target 4 of Course 1.

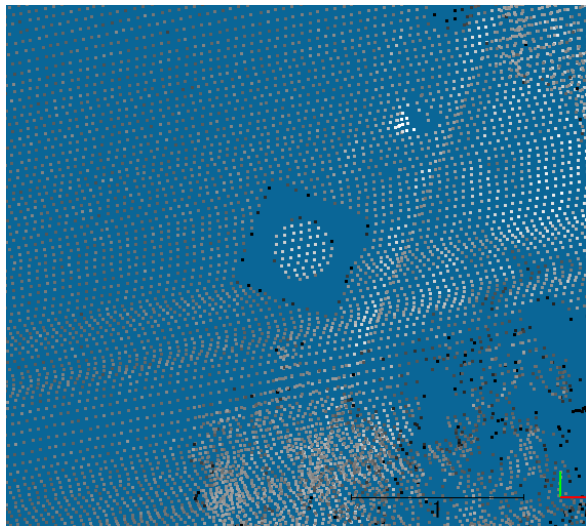


Figure 6. Target 2 of Course 1.

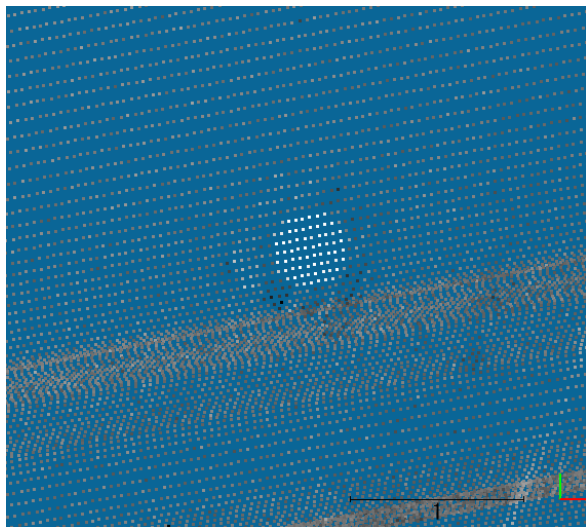


Figure 7. Target 3 of Course 1.

In addition, the point clouds with large coarseness and denseness, such as Target 3 of Course 2 shown in Figure 8, were also included, as the pitching was affected by the wind at the time of measurement.

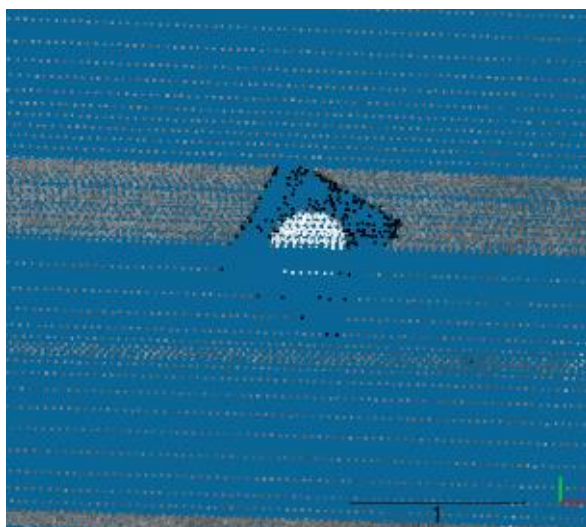


Figure 8. Target 3 of Course 2.

#### 4. PERFORMANCE EVALUATIONS

The center coordinates of the circular targets were calculated using the proposed method, as well as the weighted center of gravity and fitting circle equation methods using the points on the circumference. A manual observation was also carried out to obtain the center coordinates, and these were considered as the reference coordinates. The calculated center coordinates were evaluated qualitatively and quantitatively. The qualitative evaluation was performed by overlaying the calculated center coordinates, represented by crosses, on top of the reflection intensity of the point cloud. Figure 9 shows the results of the three methods employed for calculating the center coordinates in the stable measurement of Target 4 of Course 1 with point cloud using the reflection intensity. The crosses indicate the center of the target determined from each method: red for manual observations, green for the weighted center of gravity method, blue for the fitting circle equation method, and purple for the proposed method.

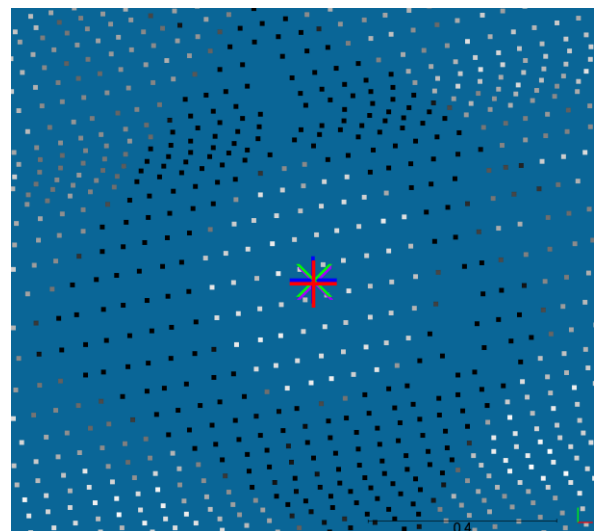


Figure 9. Center coordinates, represented by crosses, of Target 4 of Course 1.

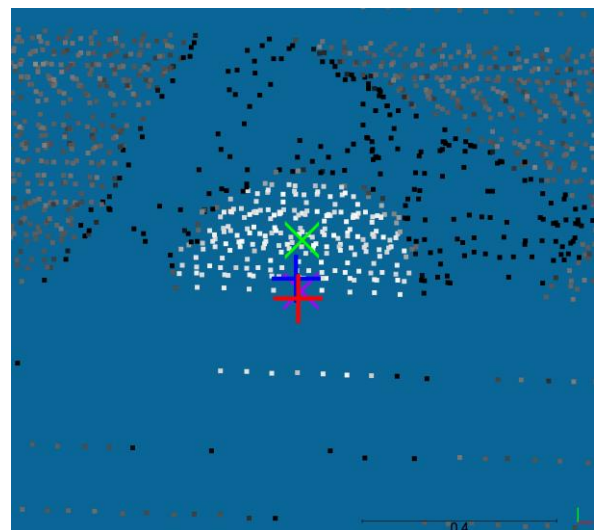


Figure 10. Center coordinates, represented by crosses, of Target 3 of Course 2 in an inhomogeneous density point cloud.

Similarly, Figure 10 shows the results of the calculation of the center coordinates of Target 3 of Course 2, including the

instances where the coarseness and denseness of the point cloud were significant.

The crosses in Figure 9, calculated for the homogeneously obtained point clouds, were almost at the same position. Thus, the difference among the processing methods were not evident in this figure. By contrast, in Figure 10, it can be recognized that the density was induced at the high-density points in the homogeneous density point cloud and that the green cross of the weighted center of gravity method was far from the red cross of the manual observation. The blue cross of the fitting circle equation method was closer to the red cross of the manual observation than to the green cross of the gravity center method, and the purple cross of the proposed method was even closer to the red one.

For performing the quantitative evaluation, the difference between the reference coordinates obtained from the manual observation and the center coordinates obtained from each method was used. The difference between the reference value and the planimetric coordinates of the center of the circular target obtained from each method was evaluated as the error distance for that method, and the results are shown in Figure 11. The different vertical axis settings for the center of gravity method and other methods are shown in the figure.

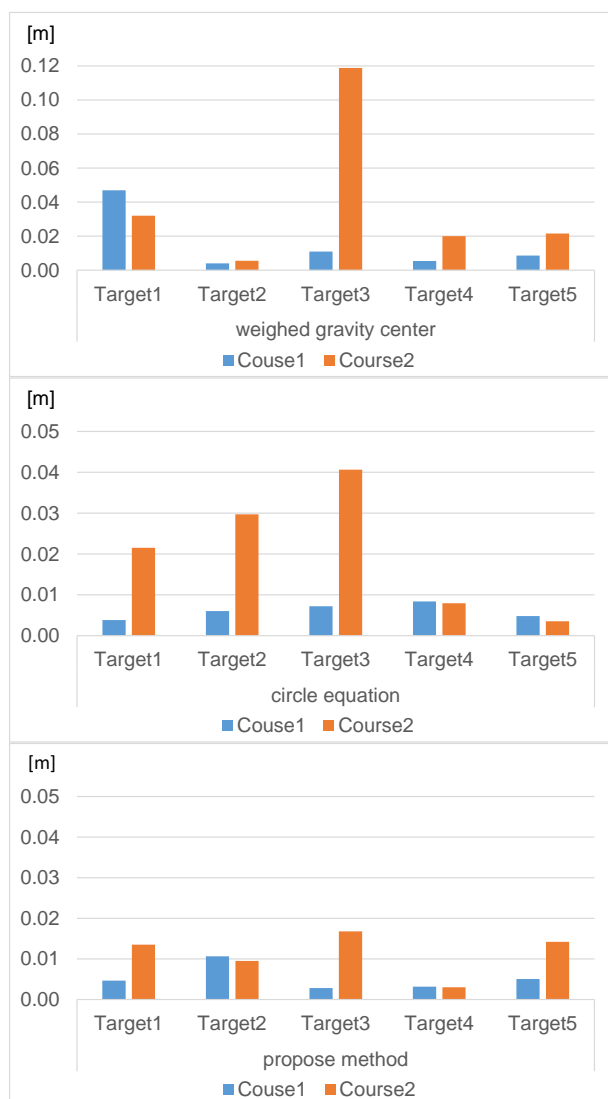


Figure 11. Error distances

For Target 4 of Course 1 of the homogeneous density measurement, shown in Figure 9, the error distances were found to be 0.005m for the weighted center of gravity method, 0.008 m for the fitting circle equation method, and 0.003 m for the proposed method. Moreover, for Target 3 of Course 2 of the measurement with a remarkable difference in density, shown in Figure 10, the error distances were found to be 0.119 m for the weighted center of gravity method, 0.041 m for the fitting circle equation method, and 0.017 m for the proposed method.

The 10 error distances obtained were averaged for each method, and the results were found to be 0.028 m for the weighted center of gravity method, 0.014 m for the fitting circular method, and 0.008 m for the proposed method. It was evident that the average of these error distances corresponded to one-fifth to one-half of the 0.045-m point intervals of the measurement plan.

Thus, it was confirmed that the proposed method did not result in prominent error distances unlike the other methods. It can be inferred that the proposed method was not affected by the bias of the point density because it used the weighted center of gravity and fitting circle equation methods to calculate the center iteratively using points near the circumference.

By contrast, the weighted center of gravity method was significantly affected by the density. The density of the point cloud and other factors were evaluated; Figures 12 and 13 show the density and point filling rate, respectively. The density in the divided area in Figure 12 was calculated by dividing the circle and adjusting the strings to equalize the area at an angle of 30° in the radial direction from the center of the circle and at variable distances from the center.

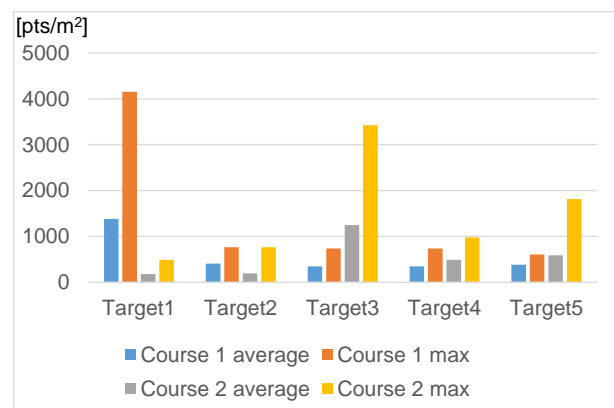


Figure 12. Density in divided area

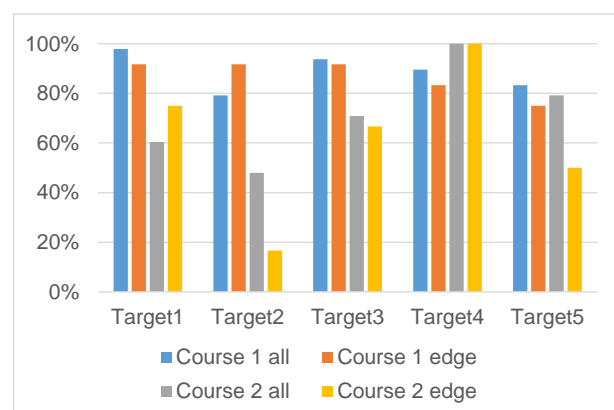


Figure 13. Point filling ratio

The maximum densities of Target 1 of Course 1 and Target 3 of Course 2 are shown in Figure 12. The coarse and dense point cloud of Target 3 of Course 2 was confirmed from Figure 10, and Target 1 of Course 1 was similarly confirmed as a coarse and dense point cloud that was obtained owing to the pitching effectiveness. The difference between the maximum and average densities was small for Target 4 of Course 1 of the stable measurement. The multiplier values of the maximum density to average density were found to be distributed from 1.6 to 4.0, and its values for Target 4 of Course 1 and Target 3 of Course 2 were 2.1 and 2.7, respectively.

The density bias was evaluated by calculating the filling ratio from Figure 13 using the number of points contained in the divided area. The filling ratio was calculated as the percentage of points contained in all of the 72 equal area divisions of the circle and at the edge of the 18 circumferences. From Figures 12 and 13, it is evident that the filling ratio of all areas and circumferences of Target 2 of Course 2 was extremely low compared to that of the other targets, and its point density was also low; however, according to Figure 11, the error distance for the weighted gravity center method was 0.006 m, which is presumed to have been caused by the small and homogeneous distribution of the points. The error distance for the fitting circle equation method of Target 2 of Course 2 was 0.030 m, which may have been influenced by the low filling ratio of the circumference. Furthermore, the error distance of Target 2 of Course 2 for the proposed method was 0.010 m. The filling ratio of Target 4 of Course 1 with the homogeneous distribution was 90% for all areas and 83% of the circumference while the filling ratio of Target 3 of Course 2 with the inhomogeneous distribution was 71% for all areas and 67% of the circumference.

It was confirmed that the difference between the homogeneous and inhomogeneous point clouds was ~20% in terms of the point filling ratio. A filling rate difference of 20% was obtained in this experiment.

## 5. CONCLUSIONS

In this paper, a method for observing the point clouds using reflection intensity was proposed for circular targets by employing a UAV equipped with a laser scanner. The proposed method, weighted center of gravity method, and fitting circle equation method were applied, and their results were compared. The data of five targets in the point cloud were acquired from two courses with a planned point density of 500 points/m<sup>2</sup>.

The center coordinates calculated using each method were evaluated qualitatively and quantitatively. The qualitative evaluation visually confirmed that the bias of the point density had a significant influence on the calculation of the center coordinates of the circular targets. A quantitative evaluation was also carried out. As a result, the average of the 10 error distances was found to be 0.028 m for the weighted center of gravity method, 0.014 m for the fitting circle equation method, and 0.008 m for the proposed method. Furthermore, the maximum error distance of the proposed method was 0.017 m, which was one-third of the 0.045-m point intervals of the measurement plan. Similarly, the average error distance of 0.008 m for the proposed method was one-fifth of the point intervals. Therefore, the observation accuracy of the point cloud using the proposed method was found to be one-fifth to one-third of the point intervals. Thus, the proposed method was able to robustly calculate the center of the circle using reflection intensity with a 20% difference relative to the homogeneous density point.

Some issues, however, still remain and require further investigation. For instance, the generality of these results was difficult to determine. As the evaluation used only one data set, it would be necessary to consider many variations. It is also unclear whether the accuracy of the relationship obtained was between the target size and point intervals. Therefore, we aim to continue this research and develop an improved understanding of the operation of UAVs equipped with laser scanners.

## REFERENCES

- Akca, D., 2003: Full automatic registration of laser scanner point clouds. *Optical 3-D Measurement Techniques VI*, 330-337.
- Belton, D. and Lichti, D. D., 2006: Classification and segmentation of terrestrial laser scanner point clouds using local variance information, *Int. Arch. Photogramm. Remote Sens. Spatial Inf. Sci.*, Vol. 36(5), 44-49.
- Cramer, M., Haala, N., Laupheimer, D., Mandlbürger, G., and Havel, P., 2018: Ultra-High Precision UAV-Based Lidar and Dense Image Matching, *Int. Arch. Photogramm. Remote Sens. Spatial Inf. Sci.*, XLII-1, 115–120. doi.org/10.5194/isprs-archives-XLII-1-115-2018.
- Csanyi, N., and Toth, C. K., 2007: Improvement of lidar data accuracy using lidar-specific ground targets. *Photogrammetric Engineering & Remote Sensing* 73(4), 385–396. doi.org/10.14358/pers.73.4.385.
- Davidson, L., Mills, J. P., Haynes, I., Augarde, C., Bryan, P., and Douglas, M., 2019: Airborne to UAS Lidar: An Analysis of UAS Lidar Ground Control Targets, *Int. Arch. Photogramm. Remote Sens. Spatial Inf. Sci.*, XLII-2/W13, 255–262. doi.org/10.5194/isprs-archives-XLII-2-W13-255-2019.
- Medić, T., Holst, C., Janßen, J., Kuhlmann, H., 2019: Empirical stochastic model of detected target centroids: Influence on registration and calibration of terrestrial laser scanners, *J. Appl. Geodesy* 13(3), 179-197. doi.org/10.1515/jag-2018-0032.
- Luhmann, T., Robson, S., Kyle, S., and Boehm, J., 2014: Close-Range Photogrammetry and 3D Imaging, 2nd edition, De Gruyter, Berlin, Germany. doi.org/10.1515/9783110607253.
- Nakano, K., Tanaka, Y., Suzuki, H., Hayakawa, K., and Kurodai, M., 2020: On Practical Accuracy Aspects of Unmanned Aerial Vehicles Equipped with Survey Grade Laser Scanners, *Int. Arch. Photogramm. Remote Sens. Spatial Inf. Sci.*, XLIII-B1-2020, 343–348. doi.org/10.5194/isprs-archives-XLIII-B1-2020-343-2020.
- Nurunnabi, A., Sadahiro, Y., Laefer, D. F., 2018: Robust statistical approaches for circle fitting in laser scanning three-dimensional point cloud data. *Pattern Recognit.*, 81, 417-431. doi.org/10.1016/j.patcog.2018.04.010.
- Otsu, N., 1979: A threshold selection method from gray-level histograms. *IEEE Trans. Syst. Man Cybern.*, 9(1), 62-66. doi.org/10.1109/tsmc.1979.4310076.